Article

Enhanced Energy Recovery in Magnetic Energy-Harvesting Shock Absorbers Using Soft Magnetic Materials

Susana Aberturas [1], José Luis Olazagoitia [2,*], Miguel Ángel García [1,3] and Antonio Hernando [1,4,5,6]

[1] Industrial Engineering and Automotive Department, Nebrija University, Sta. Cruz de Marcenado, 27, 28015 Madrid, Spain
[2] Faculty of Design and Technology, University of Design and Technology (UDIT), Av. Alfonso XIII, 97, 28016 Madrid, Spain
[3] Instituto de Cerámica y Vidrio, Campus de Cantoblanco, Consejo Superior de Investigaciones Científicas (CSIC), 28049 Madrid, Spain
[4] Instituto de Magnetismo Aplicado (IMA), UCM, ADIF, 28230 Las Rozas, Spain
[5] Donostia International Physics Center, 20028 Donostia, Spain
[6] Instituto Madrileño de Estudios Avanzados (IMDEA) Nanociencia, 28049 Madrid, Spain
* Correspondence: joseluis.olazagoitia@esne.es

Abstract: In the automobile sector, energy recovery and sustainability are becoming more and more important, and energy-harvesting suspension systems (EHSAs) have a lot of promise to improve vehicle efficiency. This investigation expands on prior work that investigated the viability of an EHSA that uses permanent magnets and amorphous core coils. The performance of the proposed system is demonstrated and enhanced in the current study through the development and optimization of a prototype. A thorough testing of the prototype is performed to determine design improvements for boosting the system's overall performance and to quantify the recovered energy. In previous work, a method was proposed to find the dependence of the magnetic flux with the relative position between the primary and secondary elements to obtain the optimal position for the system. This method is applied to optimize the energy harvesting coil by testing different configurations in terms of the placement and type of amorphous or nonamorphous core inside the energy harvesting coil. This is a crucial area of attention in order to maximize energy recovery while solving the low-frequency problem that suspension systems have (on the order of 10 Hz).

Keywords: EHSA; permanent magnets; amorphous core coils; experimental method; energy recovery

1. Introduction

The automotive industry has faced growing concerns regarding energy efficiency and sustainability in recent years, driven by the urgent need to reduce greenhouse gas emissions and reliance on fossil fuels [1]. As a response, various strategies have been developed to improve vehicle efficiency, including the implementation of energy recovery systems [2]. These systems aim to recover and reuse energy that would otherwise be lost during vehicle operation, contributing to overall fuel efficiency and a reduced environmental impact [3]. For instance, regenerative braking systems have been widely adopted in electric and hybrid vehicles, converting kinetic energy during deceleration into electrical energy to be stored and reused [4]. Similarly, energy-harvesting suspension systems have gained attention as a promising approach to recover energy from road-induced vibrations [5]. By transforming the energy generated during suspension movements into usable electrical energy, these systems can further enhance vehicle efficiency by capturing and reusing energy that would otherwise be dissipated as waste [6].

Various types of energy-harvesting suspension systems have been proposed and studied, including hydraulic, electromagnetic, and piezoelectric dampers [7].

Electromagnetic dampers have gained attention due to their potential for high energy recovery efficiency, compact design, and compatibility with existing suspension systems [8].

These dampers typically consist of a coil and a magnet, with the coil producing an electromotive force when the magnet moves relative to it, thus generating electrical energy [9]. The energy recovered can then be used to power auxiliary systems, such as lighting or electronic devices, or even to recharge the battery in electric and hybrid vehicles [3].

Despite the potential advantages, implementing efficient energy-harvesting suspension systems remains challenging. Some of the key issues include optimizing the energy conversion process, addressing the low-frequency nature of suspension systems (typically around 10 Hz), and minimizing the impact on ride comfort and road handling [10]. Additionally, further research is needed to identify suitable materials and designs that can maximize energy recovery while maintaining durability and reliability in real-world conditions.

In the quest for improved vehicle energy efficiency, several energy-harvesting suspension system (EHSA) designs have been proposed and studied in the literature, each with its unique advantages and drawbacks. This section provides a brief review of these approaches, highlighting their strengths and limitations, and emphasizing the need for new, innovative solutions.

Hydraulic EHSA: Hydraulic energy-harvesting dampers involve the use of a hydraulic pump and motor to convert the mechanical energy generated by suspension movements into electrical energy [5]. The primary advantage of hydraulic systems is their ability to handle high forces and displacements, resulting in potentially high energy recovery rates [11]. However, these systems tend to be bulky, complex, and may suffer from fluid leakage and maintenance issues. Additionally, the efficiency of hydraulic energy recovery is highly dependent on the damping coefficient and the design of the pump and motor, which can be challenging to optimize.

Electromagnetic EHSA: As mentioned earlier, electromagnetic dampers have gained considerable interest in recent years. These systems employ a coil and a magnet to generate electrical energy through electromagnetic induction, offering advantages such as a compact design, compatibility with existing suspension systems, and a potentially high energy recovery efficiency [12]. However, challenges remain in optimizing the energy conversion process, addressing the low-frequency nature of suspension systems, and minimizing the impact on ride comfort and road handling.

Piezoelectric EHSA: Piezoelectric energy-harvesting dampers utilize piezoelectric materials to convert mechanical energy into electrical energy through the piezoelectric effect [13]. These systems are lightweight, compact, and have the potential for high energy conversion efficiency. However, they tend to be more suitable for applications with high-frequency vibrations, as the energy recovery efficiency decreases significantly at low frequencies, such as those typically encountered in suspension systems. Additionally, the need for complex power-conditioning circuits and the relatively high cost of piezoelectric materials can be limiting factors for the widespread adoption of piezoelectric EHSAs [14].

Despite the progress made in the development of EHSAs, there remains significant room for improvement in terms of energy recovery efficiency, durability, and cost-effectiveness. Consequently, there is a need for innovative solutions that address the challenges and limitations, such as the simultaneous application of hard and soft magnetic materials in electromagnetic dampers. By exploring new materials, designs, and control strategies, researchers can potentially develop more efficient and practical EHSAs that contribute to the broader goal of sustainable transportation.

Innovative solutions, such as the proposed simultaneous application of hard and soft magnetic materials in electromagnetic dampers, hold the potential to overcome these limitations and pave the way for more effective energy-harvesting suspension systems. By exploring novel materials, designs, and control strategies, researchers can push the boundaries of current technologies and contribute to the development of more efficient, durable, and cost-effective EHSAs that are well-suited for real-world applications.

Magnetic energy-harvesting shock absorbers (EHSAs) have emerged as a promising approach for recovering energy from suspension systems, employing permanent magnets and coils to generate electrical energy through electromagnetic induction [15]. This section

reviews the design of magnetic EHSAs, discussing the advantages and limitations of various configurations, as well as identifying research opportunities in the literature.

Linear electromagnetic EHSAs: In this design, a coil is wound around a tubular structure, while a permanent magnet is attached to the piston of the damper, which moves linearly within the coil [16]. When the suspension undergoes vibrations, the relative motion between the magnet and the coil induces an electromotive force, generating electrical energy. Linear electromagnetic EHSAs offer the advantages of a simple design, compatibility with conventional suspension systems, and a potentially high energy recovery efficiency. However, they face challenges in optimizing the energy conversion process.

Rotary electromagnetic EHSAs: Rotary designs convert the linear motion of the suspension system into rotational motion, which drives a generator to produce electrical energy. Various forms of rotational electromagnetic dampers exist. Given that vehicle suspensions engage in translational movement, the creation of a rotationally variable magnetic field necessitates a mechanism that transforms this translational motion into a rotational one. There are several well-established systems that achieve this conversion, including rack–pinion [17], hydraulic systems [18], ball-screw mechanisms [19], and even more unconventional methods such as the "Screw Linkage Mechanism" [20], "Two-Leg Motion" [21], or those utilizing a flywheel drive [22]. Each of these systems comes with its own set of equivalent inertias, backlashes, and frictional forces that can influence the dynamic behavior of the shock absorber, and consequently, the vehicle's overall performance. Rotary electromagnetic EHSAs can offer a higher energy conversion efficiency than linear designs, particularly at low frequencies, due to the increased mechanical advantage provided by the conversion mechanism. However, the complexity of the mechanical linkage may introduce additional friction losses, reduce reliability, and increase manufacturing costs.

Both linear and rotary magnetic EHSAs have demonstrated the potential for energy recovery from suspension systems, but several challenges remain. Key areas of ongoing research include the optimization of magnet and coil configurations, the development of advanced materials, and the integration of energy-harvesting systems with active suspension control strategies. For instance, the use of hard and soft magnetic materials, as well as amorphous cores in the coil, can potentially enhance energy recovery and overcome the limitations associated with low-frequency operation. Furthermore, the exploration of novel geometries and coil designs may lead to a more efficient energy conversion and reduced impact on ride comfort and handling.

In conclusion, magnetic EHSAs represent a promising avenue for improving vehicle energy efficiency, with both linear and rotary designs offering unique advantages and opportunities for further research. By addressing the challenges and limitations of current EHSA designs, researchers can contribute to the development of more efficient, durable, and practical energy-harvesting suspension systems that pave the way for a more sustainable future in transportation.

In conclusion, energy-harvesting suspension systems have gained significant attention in recent years as a promising avenue for improving vehicle energy efficiency and promoting sustainability in transportation. Various approaches, including hydraulic, electromagnetic, and piezoelectric dampers, have been explored and studied in the literature, with each offering unique advantages and challenges. However, existing designs have yet to fully address the demands of low-frequency operation, high energy recovery efficiency, and minimal impact on ride comfort and road handling.

The state of the art reveals a need for innovative solutions to overcome these limitations and optimize energy recovery in suspension systems. The novelty proposed in this article, focusing on the simultaneous application of hard and soft magnetic materials and the optimal positioning of an amorphous core within the coil, has the potential to address some of the challenges faced by current magnetic EHSAs, particularly in the context of low-frequency operation.

In a previous article [9], the feasibility of the system was studied, specifically presenting an experimental method to maximize energy recovery by defining the optimal

relative position between the primary element (magnet) and the secondary element (energy-harvesting coil). In this article, a prototype is developed to demonstrate and optimize the functioning of the proposed system as a concept. Tests are conducted with the prototype to obtain not only energy recovery results but also conclusions regarding design improvements aimed at optimizing the demonstrator system. Additionally, the optimal shape and position of the amorphous core in the energy-harvesting coil are studied in detail to recover the maximum energy and address the challenge posed by the low operating frequency of a suspension system (on the order of 10 Hz).

Furthermore, the use of NdFeB magnets in the proposed system aligns with the European Union funded REMANENCE initiative (Rare Earth Magnet Recovery for Environmental and Resource Protection), promoting the reusability of these critical materials and contributing to environmental sustainability [23]. The article presents experimental data from the prototype testing, images of the fabricated prototype, and conclusions drawn from the obtained results.

The electromotive force, EMF, induced in the pick-up coil becomes the relevant parameter on the basis of the electromagnetic damping process. In this article, we study the influence of a ferromagnetic coil nucleus on the induced EMF in a coil subject to an alternating exciting magnetic field with a fixed amplitude and frequency. Instead of an oscillating magnet, we use a small coil fed by an AC source, as explained along the next paragraphs. In fact, as thoroughly discussed below, an oscillating magnet or an AC current coil are not equivalent in many physical aspects, but both generate a time-dependent flux through the pick-up coil that enables us to study the influence of the ferromagnetic nucleus. Moreover, the control of the time-dependent flux can be more easily achieved by using a coil.

To understand the starting point of the present article, it is useful to know the previous study that was carried out on this topic and published in [9]. In that previous work, an experimental method was proposed to obtain the dependence of the flux variation through a coil according to the relative position between the primary and secondary elements.

$$EMF = -d\phi/dt \tag{1}$$

The previous equation shows that, in order to calculate the electromotive force or flux variation of the secondary coil, in the case of a primary coil supplied with AC current, it is enough to know how the flux varies with time. However, when we have a magnet or a primary coil connected to DC current and in motion, which is equivalent in both cases to having a fixed oscillating current, the flux will be caused by the variation of the relative distance between the primary and secondary elements.

$$\frac{d\phi}{dt} = \frac{d\phi}{dz}\frac{dz}{dt} = \frac{d\phi}{d(r - r\prime)}\frac{d(r - r\prime)}{dt}\alpha\phi(r - r\prime) \tag{2}$$

z being this relative distance, expressed as $(r - r\prime)$, to obtain $\frac{d\phi}{dt}$, it is necessary to know the dependence $\phi(r - r\prime)$. To obtain this dependence in an analytical way it is necessary to solve very complex calculations. This complexity is noticeable for example in the flux calculation shown below. To calculate the magnetic flux through the secondary coil, it is necessary either to know the value of the perpendicular component of the magnetic field at all points on the surface of the coil, or to find the circulation of the potential vector (A) along the contour C of the secondary coil.

$$\phi = \int B \cdot ds = \oint_C A \, dl \tag{3}$$

If *A* is the vector potential created by a primary coil, the value of the vector potential of a point at the primary coil must be calculated for each point on the secondary coil, using the following equation.

$$A_{coil} = \mu_0 \int_1 \frac{I \cdot dl}{r} \tag{4}$$

Therefore, the flux through the secondary coil would be as follows:

$$\phi = \oint_C \mu_0 \oint_1 \frac{I \cdot dl_1}{r_2 - r_1} dl_2 \tag{5}$$

If the vector potential *A* is created by a magnet, its corresponding expression becomes:

$$A_{magnet} = \frac{mxr}{4\pi(r_2 - r_1)^3} \tag{6}$$

Note that these parameters (*A* and ϕ) are time-dependent functions, which adds some difficulty.

In summary, as is known, in a coil with a contour *C*, the flux is the integral along *C* of the vector potential *A*, and the calculation of both this integral and its integrand is often tedious. Particular methods can be used to solve this problem, including a finite element calculation or the method proposed in the paper [9] summarized below.

Given the complexity of the previous calculations, it was decided to develop an experimental method, with which it was observed that taking measurements with a magnet–coil system is of high complexity and low accuracy in the data obtained; therefore, a method able to achieve the intended objective was proposed, using a coil–coil system.

To find the optimum position between the primary and secondary elements with which the maximum energy, i.e., the maximum induced electromotive force, is obtained, it is important to understand that:

(i)   If the flux variation is to be obtained with a fixed coil, fed by AC current, the optimum position to achieve, at a fixed current intensity and frequency, a maximum induced electromotive force is the position of maximum flux.

The current flowing through the primary coil is given by the following expression:

$$I(t) = I_0 \cos \omega_1 t \tag{7}$$

The position of the maximum flux is given with coaxial coils and the minimum distance between them (*z* = 0), as shown in Figure 1 below.
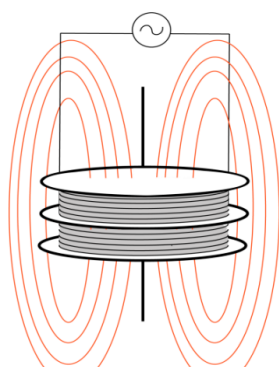

Figure 1. Position of maximum induced EMF for the case of a primary coil with AC current.

(ii)   If the flux variation is to obtained by the movement of the source, magnet, or coil, with respect to the secondary coil, the worst position is that of the maximum flux, because, by definition of the maximum, if the flux is maximum for a determined position of the source, x, the derivative of the flux with respect to x is annulled at that point and

therefore the electromotive force induced by the displacement of the source (variation of x) is zero.

The movement of the source oscillating in the *z*-axis, around the point *z** with amplitude z_0 and oscillation frequency ω_2 can be expressed as follows:

$$z(t) = z^* + z_0 \cos \omega_2 t \tag{8}$$

These concepts are shown through equations in Table 1:

Table 1. Magnetic field and electromotive force expressions.

	CASE 1 AC Coil–Coil System	CASE 2 DC Coil–Coil System [1]
Magnetic field equation	$B(z, r, t)$ $B = \mu_0 I(t) f(z, r)$	$B(z(t), r)$ $B = \mu_0 I f(z(t), r)$
Flux equation	$\phi = N\mu_0 I_0 \cos(\omega_1 t) \iint f(z, r) ds$ $\phi = N\mu_0 I_0 \cos(\omega_1 t) g(z, r)$	$\phi = N\mu_0 I \iint f(z(t), r) ds$ $\phi = N \mu_0 I g(z(t), r)$
EMF equation	$EMF = -\frac{d\phi}{dt}$ $EMF = N \mu_0 I_0 \omega_1 \sin \omega_1 t g(z, r)$	$EMF = -\frac{d\phi}{dt}$ $EMF = N\mu_0 I \omega_2 z_0 \sin \omega_2 t \frac{dg(z, r)}{dz}$

[1] Basis of the proposed method.

It is possible to understand statements (i) and (ii) through the equations of the previous table focusing attention on the term $g(z, r) = \iint f(z, r) ds$, and knowing that this term expresses the relative position between the primary and secondary elements, it is observed that:

In the AC coil–coil system, both the flux and the *EMF* are directly proportional to the term $g(z, r)$, so the *EMF* is maximum at the same point where the magnetic flux is. However, in the DC coil–coil system, the flux is proportional to the $g(z, r)$ term while the *EMF* is proportional to the derivative of that term, $\frac{dg(z, r)}{dz}$. When $g(z, r)$ is maximum, by definition, its derivative is zero $\frac{dg(z, r)}{dz} = 0$.

After defining the method, experimental measurements of induced electromotive force and its gradients were taken, in order to find the maximum gradient, for different relative positions of the system. The optimum position was the one corresponding to having the secondary coil oriented horizontally (Figure 2) and with a height difference with respect to the primary element (A, B in the next scheme) of 3 cm. In that position, the maximum gradient was obtained more specifically in the section where the secondary coil moved from position C = 0.5 cm to C = 1 cm.

The results and conclusions of that first paper were taken as a starting point for the second part of the investigation. Using the demonstrator manufactured for this article, and the knowledge obtained from it about the optimum relative position between the primary and secondary elements, we also tried to optimize the secondary element, the energy collector coil. In order to improve the efficiency of the conversion into electromagnetic energy, the influence of a ferromagnetic nucleus was analyzed by using amorphous ferromagnetic ribbons with different relative positions with respect to the secondary coil. For this study, a theoretical study and some experimental tests were carried out.

It should be noted that the induced voltage in the case of an oscillating magnet with a fixed amplitude and frequency serves as a useful indicator of the potential power that can be harnessed from our system. There is a direct proportionality between the usable power and the square of the collected voltage; it is known that the maximum of the obtained power is achieved when the value of the load resistance is equal to the resistance of the secondary coil. However, the interest of this article is focused not in obtaining the maximum power but in inquiring about the maximum induced voltage.
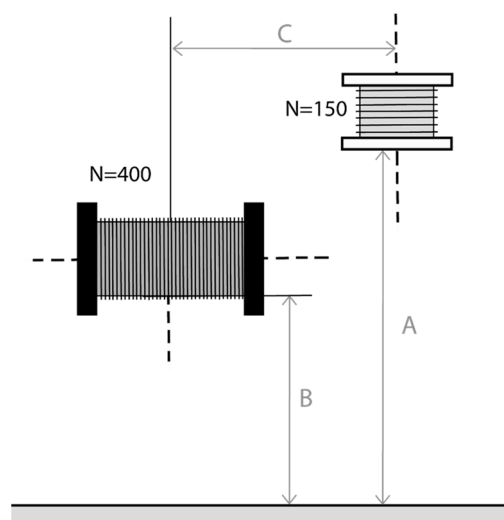
Figure 2. Diagram with parameters A, B, and C to vary the relative positions between primary and secondary coils during tests (N = number of spires in each coil).

2. Theoretical Approach

Until now, in the tests carried out in the first paper, the input used was a 1 kHz frequency signal, a much higher frequency than the one that the real system would have, so the results of the energy recovered were not quantitatively significant since they were not taken in real conditions. The real frequency generated by the suspension movement produced by the irregularities of the road in a vehicle is of the order of 10 Hz. The reason why such a high frequency was used in the tests is that at a low frequency, the energy recovered by the collector coil is almost insignificant. This is the origin of the problem to be solved in this section: it is necessary to optimize the system to increase the energy recovered from a frequency of the order of 10 Hz, which means that the output (energy obtained) must be multiplied without varying the input conditions (frequency). To do this, it is necessary to study the various ways in which it is possible to multiply the flux through the coil and implement those that optimize the system.

This problem can be divided into two different parts, focusing on the one hand on the multiplication of flux through the primary or inductor system and, on the other hand, through the secondary or induced system.

In the case of optimizing the primary system, some of the possibilities would be to increase the size of the magnets, increase their number, or vary their positions, but these are simple proposals that should be studied in detail.

In terms of optimizing the secondary system, namely, the collector coil, several strategies may be considered: increasing the number of turns in the coil, connecting multiple coils in series, and/or employing a core made of amorphous material. This article primarily focuses on optimizing the system through modifications to the secondary element, specifically by using an amorphous core.

Amorphous material consists of alloys of ferromagnetic materials with metalloids, such as Fe, B, Si, whose properties are due to the "disorder" of their atomic dipoles. The characteristic of interest of these materials for flux multiplication in the coil is magnetic permeability.

The effect of flux multiplication produced by a ferromagnetic nucleus of the pick-up coil increases with the magnetic permeability; therefore, it is necessary to use materials with a high permeability so that with a low external field H, the magnetic flux density is high. For our application, as the field is changing over time, in addition to a high permeability it is necessary that magnetic losses are as low as possible.

The real part of the magnetic permeability should be as high as possible in order to multiply the flux. This real component is inversely proportional to the magnetic anisotropy that, in metallic glasses, vanishes in the first order due to the random orientation of the

local easy axes. An additional requirement rises when the exciting field and thereby, the magnetic flux, changes with time at a given frequency. In this case, to save energy, the losses should be low, but losses are reflected in the imaginary component of the permeability that is proportional to the anisotropy, magnetostriction, and electrical conductivity of the nucleus. These losses can come from the hysteresis cycle, proportional to the frequency, and/or from Eddy currents, proportional to the square of the frequency. Amorphous or metallic glasses [24] are ideal for both; as they have negligible magnetic anisotropy and low conductivity, they exhibit a high real permeability and an extremely low imaginary component since the losses due to eddy currents, proportional to the conductivity, as well as those due to hysteresis, proportional to the anisotropy, are also low.

The ribbons used in this article were ferromagnetic amorphous alloy manufactured by rapid solidification at a speed of approximately 10^6 K·s^{-1}. The brand name of this material is Metglas MBF-15, and its chemical composition is $Ni_{76.5}Fe_{4.2}Cr_{13}B_{2.8}Si_{45}$. Such material has moderate magnetic properties, but it is mechanically outstanding thanks to its flexibility and ductility, relevant properties for constructing a robust device. It is characterized by a low positive magnetostriction constant (10^{-6}), low saturation magnetization (0.5 T), and a value of the complex permeability that remains constant up to 10 kHz [25]. As is shown in [25], the main source of losses, contributing to the imaginary component of the permeability in metallic glasses, comes from the magnetoelastic coupling. This mechanism starts to be effective at frequencies close to the first extensional elastic mode of the ribbon, which, for a length of a few centimeters, is above 10 kHz. These properties, besides its low cost, makes Metglas MBF-15 a suitable compound to obtain the general aspects of how reliable the application of amorphous core might be in energy-recovering devices. However, further research and experiments oriented to elucidate a more appropriate material, from a magnetic point of view, should be carried out. For example, using higher-saturation-magnetization Fe-rich compounds or low-magnetostriction cobalt-rich-based alloys or applying suitable stress relief annealing to magnetostrictive iron–nickel alloys. As is well known, these types of samples are outstanding as concerns losses reductions [26–28].

It is possible to produce amorphous materials of different geometries, in particular, microwires and thin ribbons. For the experiments conducted in this research, we elected to use ribbons for the amorphous core of the coil instead of other options, such as microwires. The main reason for this decision was rooted in the ease of designing a reel and coil around a rectangular ribbon core as opposed to microwires, given the materials available in our laboratory. Furthermore, using ribbons allowed us to completely fill the core that encapsulates the coil, thereby preventing any air from remaining within the core. In the case of using thin rectangular ribbons of amorphous material, the orientation and thickness of the ribbon is important, as well as the number of ribbons used.

For a given charge density, as the distance between poles of different signs increases, the demagnetizing field H becomes smaller. This means that the longer the length of the ribbon, the lower its demagnetizing field, as shown in the next figure, in which the arrows with a dashed line represent the demagnetizing field and the arrows with a continuous line represent the magnetization of the material itself (Figure 3).

Below, the scheme of the amorphous film core coil that is used as an energy-recovery element in the tests of the present research is shown (Figure 4).

Regarding the thickness of the ribbons, they should have a small thickness in order to maintain the amorphous structure during the cooling process. Moreover, the thicker they are, the greater the eddy currents (Foucault currents) are, which produce energy losses in the form of heat (Joule effect).

However, in order to enhance the magnetizing effect of the ribbons, many identical films are placed stacked on top of each other, forming a kind of block (Figure 5). This way, as the surface area crossed by the magnetic field increases, the flux increases, but

at the same time, as the surface area increases, the magnetization is decreasing by the magnetization effect.

$$\phi = \int B \cdot ds = \mu_0 H_1 \cdot S + \mu_0 M \cdot S' + \mu_0 H_2 \cdot (S + S\prime) \tag{9}$$

$$\text{———} \quad M$$
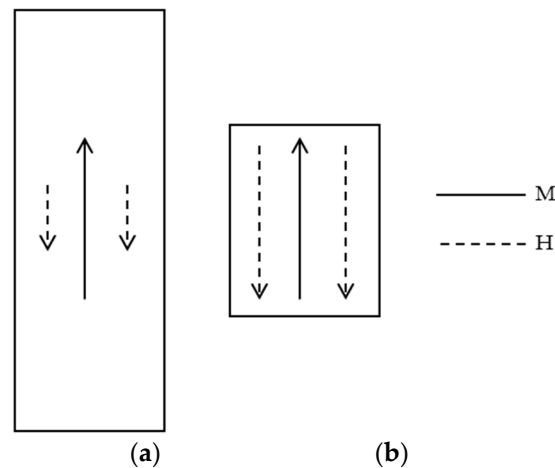$$\text{- - - - -} \quad H$$

(**a**) (**b**)

Figure 3. Films of amorphous material with different dimensions. The sheet (**a**) has a large distance between the poles, and therefore a weaker coercive field. The (**b**) film, as it has a smaller distance between the positive and negative poles, has a stronger coercive field that can cancel the magnetic effect of the material (M).

Figure 4. Coil with amorphous material core.

Figure 5. Geometry of the coil and core amorphous film assembly.

At the same film magnetization, the flux increases when increasing the surface S' (thickness, adding more films), because the term $\mu_0 M \cdot S'$ increases. At the same time for

an applied field H_1, as $S\prime$ increases, the magnetization decreases because the opposite sign term $\mu_0 H_2 \cdot (S + S\prime)$ increases, and one can reach a point where the demagnetizing factor demagnetizes the set. That is, there is a competitive effect; on the one hand, increasing the section increases the flux supposing a constant magnetization and on the other hand, increasing the section decreases the magnetization for a given applied field as the demagnetizing field increases as a function of S/L, where S' is the section or the secondary coil that is bigger than S, the width of the magnetic core (thickness of the set of ribbons) and L is the length of the laminates (distance between poles).

Moreover, as it is known, the longer the length of the laminates, the more of them can be stacked, as the demagnetizing factor depends on the ratio indicated in the previous equation. This compromise between the section of the set of laminates and their length would be another point to be studied in future research.

Relative Position of the Coil to the Amorphous Core Material

To continue with the optimization of the secondary element, a theoretical study about the optimum relative position of the coil with respect to the amorphous core was carried out. For this study, an AC coil was used as the primary element because of the facility for varying the parameters and observe the results [9].

A uniform and longitudinally magnetized elongated body, such as a thin sheet of great length, was used for this purpose. The external magnetic field applied to this film produces poles at the ends of the film, the south pole being where the magnetization is born and the north pole where it dies. These poles also create a demagnetizing H field inside the film that goes from north to south (field in the opposite direction to the magnetization).

In the demagnetizing factor approximation, this field H inside the film is usually considered uniform, as if it were a capacitor; however, the reality is that it is not uniform but is more intense near the poles than at the midpoint between them, as the surface area of the poles is much smaller than the distance between them. Thus, it would be more accurate to approximate the system with 2-point charges, one positive and one negative, separated from each other by a distance equal to the length of the film, L.

The approximation of the demagnetizing factor to a capacitor would be more suitable if the film in question were transversely magnetized, so that the distance between the plates of the capacitor would be the thickness of the film, e (Figure 6).
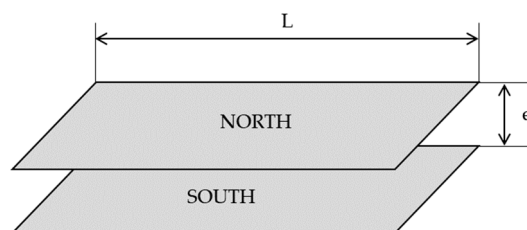

Figure 6. Transversely magnetized film of thickness e, taken as plates of a capacitor.

The equation that defines the B field inside the secondary system (region of the coil with amorphous core) is expressed as follows:

$$B_{iinternal\ secondary\ coil} = \mu_0 H_1 + \mu_0 H_2 + \mu_0 M_2 \tag{10}$$

The magnetic field B outside the coil is described below:

$$B_{external\ secondary\ coil} = \mu_0 H_1 + \mu_0 H_2 \tag{11}$$

where:

H_1 = field created by the primary system composed in this case of a coil through which circulates an AC current. If a field is applied on the secondary, H_1 decreases as the secondary moves away from the primary system.

H_2 = field created by the magnetization or magnetized matter. This field inside the material is called the demagnetizing field, and outside, it is called the magnetic field created by a magnet.

M_2 = magnetization of the secondary system, which depends on H_2.

Therefore, the field H_2 lies along the opposite direction to both H_1 and M. The field that magnetizes matter in the case of an amorphous material core is $H_1 + H_2$, except if the core were an infinite long wire, in which case there would be no demagnetizing field (the poles that are created at infinity are too far from each other).

The film of amorphous material is used to multiply the flux, i.e., with a very small value of H_1 a very large value of M is obtained. When having the core of amorphous material in the coil, most of the voltage induced in the system is due to the magnetization of the material, not to H_1, since $M \gg H_1$.

The value of the electromotive force is the derivative of B with respect to time, as indicated in the second row of equations in Table 2. Keeping the number of amorphous material films constant, when varying H_1, the value of the magnetization M varies and therefore, the value of the derivatives.

Table 2. Derivative of the magnetic *B* field, comparison between air and amorphous material core.

Magnetic Field B and Electromotive Force on the Secondary	
If the Core of the Secondary Coil Is Air	**If the Coil Core Is Amorphous Material**
$B = \mu_0 H_1$	$B = \mu_0 H_1 + \mu_0 H_2 + \mu_0 M$ [1]
$EMF = \frac{dB}{dt} = \mu_0 \frac{dH_1}{dt}$	$EMF = \frac{dB}{dt} = \mu_0 \frac{dH_1}{dt} + \mu_0 \frac{dH_2}{dt} + \mu_0 \frac{dM}{dt}$
	Where $M \gg H_1$

[1] In this case, B is much larger due to the term $\mu_0 M$, and therefore, so is the *EMF*. The collected induced voltage signal is higher with a core of amorphous material than with air.

This proportional relationship of H_1 and M has an exception when the material is magnetized at saturation. In that situation, although the secondary system moves away from the primary (H_1 is decreasing), the secondary system is still magnetized in the same way because the major contribution comes from the magnetization of the amorphous material, and this magnetization M remains constant in the case of being magnetized at saturation.

Once this difference between using air and amorphous core material has been established, a second order of approximation can be made; depending on the position of the secondary coil with respect to its amorphous core (Figure 7), the demagnetizing field, i.e., the factor $\mu_0 H_2$, will vary.
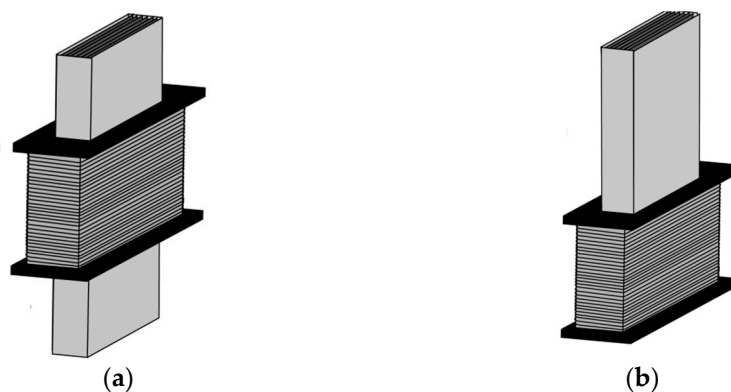

(a)   (b)

Figure 7. Secondary coil with amorphous core material: (**a**) secondary coil centered with respect to the core of amorphous material; (**b**) secondary coil off-center with respect to the amorphous material core.

As seen in the previous paragraphs, as the secondary system moves away from the primary, H_1 and M decrease. On the other hand, the field H_2 (created by magnetization) decreases with M, but its value is not constant over the entire surface of the amorphous material; it is more intense at the poles of the sheet than at the center or midpoint between the poles, and it is not homogeneous. Thus, there may be a moment when the magnetization disappears because H_2 at the edges is equal to H_1, that is, H_1 has reduced its value so much when moving away that it is equal to H_2; in that situation, there is no magnetization at the edges, and the material is demagnetized. As H_2 is larger at the edges than in the center, it is to be expected that the system with the coil at the edge of the film will be demagnetized earlier than the system with the coil at the center of the film.

To summarize, the magnetization of the film, although it can reach the saturation in its central part after a certain value of H_1, could be much less magnetized at the ends since the real field acting on them would be lower than in the center. In the center of the sample, the field due to the primary element and the magnetization is:

$$B = \mu_0 H_1 + \mu_0 H_2 \tag{12}$$

This field is enough to magnetize at saturation. However, at the extreme, the field is:

$$B\prime = \mu_0 H_1 + \mu_0 H_2\prime \tag{13}$$

Moreover, H_2' is higher in absolute value than H_2, as the demagnetizing fields are opposite to H_1; it is observed that the effective field in the center is higher than at the ends, and therefore, in a certain position, the film can be magnetized in the center and not at the ends.

Plotting the expression of the electromotive force collected by the secondary coil as a function of the distance between the primary and secondary systems, for the cases in which the coil is centered with respect to the amorphous core and off-center (at the end of the film), we obtain Figure 8, which can be used as a simulation of what would be obtained in an experimental test.
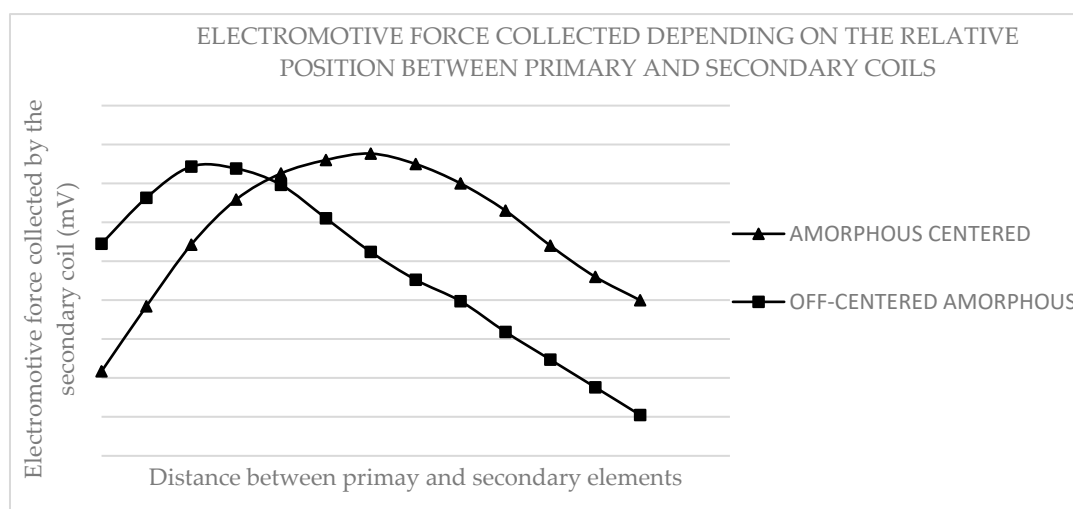

Figure 8. Comparison of electromotive force between centered and off-center coil with respect to the amorphous core.

If the secondary coil is positioned in the center of the amorphous ribbon, the resulting signal differs from when the coil is situated at the edge of the ribbon. In the latter scenario, the field collection occurs in an area where the demagnetizing H-field is more intense than in the center of the ribbon.

Assuming a uniform applied field H_1 (generated by the primary), the magnetization at the ends of the ribbon will be weaker. Consequently, with the same H_1, the B field at the ends will be smaller than at the center, resulting in a lower induced voltage at the ends. This is the reason why as the position of the secondary coil changes, the induced voltage decreases more rapidly when the coil is situated at the edge of the ribbon.

H_1 and M_2 are equal both in the case where the coil is in the center of the film and in the case where it is located at one of the ends. However, the demagnetizing field of the H_2 film varies according to the position in which it is taken, where $H_2 < H_2\prime$ and therefore, $B > B'$.

Given that the signal is primarily a result of magnetization, and that the H_2 field is smaller at the center, the secondary system will reach magnetization saturation regardless of its position. This happens because the demagnetizing field is minimal for each position assumed by the ribbon. As such, it is expected that the graph showing the *EMF* collected by the secondary coil as a function of position will exhibit a later drop when the coil is placed at the end of the ribbon. Table 3 shows the equations of the *EMF* in each case.

Table 3. Magnetic field's derivative B: comparison between centered and off-center coil of the amorphous core.

Derivative of the Magnetic Field as Function of Time	
Coil Centered with Respect to the Amorphous Core (Amorphous Centered)	**Off-Center Coil with Respect to the Amorphous Core (Amorphous off-Center)**
$B = \mu_0 H_1 + \mu_0 H_2 + \mu_0 M_2$ $EMF = \frac{dB}{dt} = \mu_0 \frac{dH_1}{dt} + \mu_0 \frac{dH_2}{dt} + \mu_0 \frac{dM_2}{dt}$ Where $M_2 \gg H_1$	$B' = \mu_0 H_1 + \mu_0 H_2' + \mu_0 M_2$ [1] $EMF\prime = \frac{dB}{dt} = \mu_0 \frac{dH_1}{dt} + \mu_0 \frac{dH_2'}{dt} + \mu_0 \frac{dM_2}{dt}$ Where $M_2 \gg H_1$

[1] In this case, B is much bigger due to the term $\mu_0 M$, and so is the *EMF*. The collected induced voltage signal is higher with a core of amorphous material than of air.

3. Experimental Approach and Discussion

Two coils were used, a circular coil of 150 spires and a rectangular coil of 300 spires. The circular coil was the primary system, so it was connected to a function generator with a frequency of 1 kHz and a peak-to-peak voltage of 5 V (Figure 9). The rectangular coil was the secondary system which was connected to the lock-in to show the voltage values induced in the secondary, as shown in Figure 10.
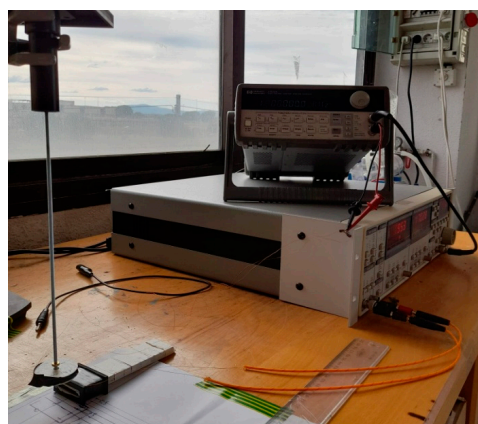

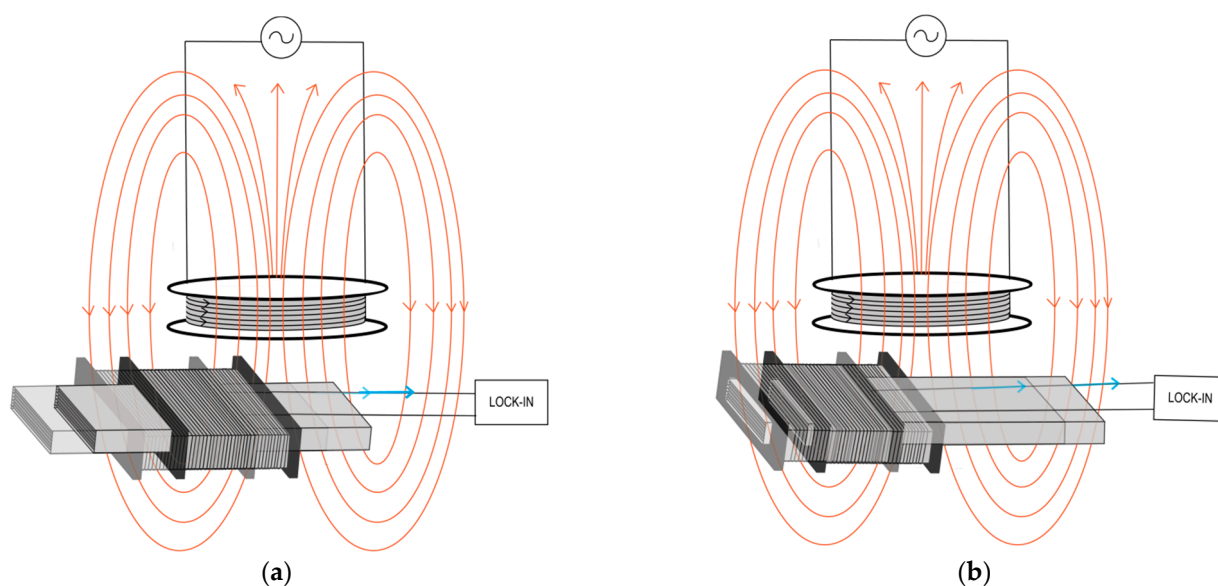**Figure 9.** System to be tested and measuring devices.

Figure 10. Scheme of the amorphous core coil system tested showing the 2 systems whose induced electromotive force was measured in the secondary: (**a**) test with centered amorphous core material; (**b**) test with off-center amorphous core material.

The measuring device (lock-in) used was very sensitive, so the data obtained could change with position variations of 1 mm, inclinations, devices located around it, and environmental conditions in general. For this reason, in order to obtain reliable data, three measurements (P1, P2, P3) were taken for each system with the same core and the same positions.

First, the data of the recovered electromotive force were collected for the secondary coil system with an air core. Then, the same test was repeated but adding the amorphous core to the secondary coil. In order to go one step forward and understand better the influence of the amorphous material on the test, two amorphous core systems were defined, which differed in the position of the amorphous material with respect to the coil.

In Figure 11, the electromotive force induced in the three cases is represented; it shows the difference in the magnitude of the electromotive force for the same position of the coils according to the core of the energy-collecting coil.

As can be seen, not only the magnitude of the induced electromotive force varied, but also the shape or trend of the graphs for each of the three models. On the one hand, in the case of the curves shown in Figure 11 corresponding to the air core, the maximum electromotive force was reached in a position such as in the case of the off-centered amorphous core material, and from this peak, the voltage collected decreased.

In this decreasing region, the observed reduction in the electromotive force was quite higher in the case of the off-center amorphous core, in comparison with the case of the air core in which a smooth progressive decrease was observed.

The graphs representing the centered amorphous core case took longer to reach the maximum voltage and remained at values very close to the maximum for a longer interval of positions.

When the gradients of the three cases tested were compared, a great difference was observed between the air-core coil test and the two tests with an amorphous material core; the variation of the electromotive force collected by the secondary being much higher in the case of the latter two.

When the gradient of these tests was calculated and plotted (Figure 12), it was possible to observe more clearly which case presented the maximum value of the gradient, which was the objective of that test, since the maximum gradient corresponded to the maximum

variation of the induced electromotive force and consequently, to the maximum energy collected by the secondary element of the system (maximum energy recovered).
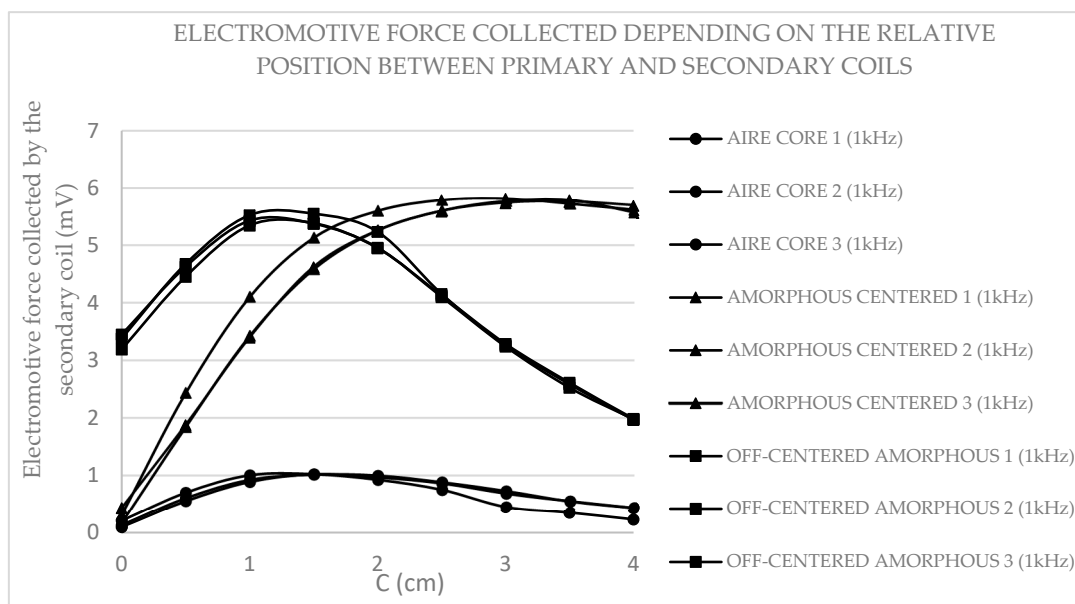

Figure 11. Induced electromotive force varying the relative position between primary and secondary coils for 3 different cores in the secondary coil at 1 kHz.
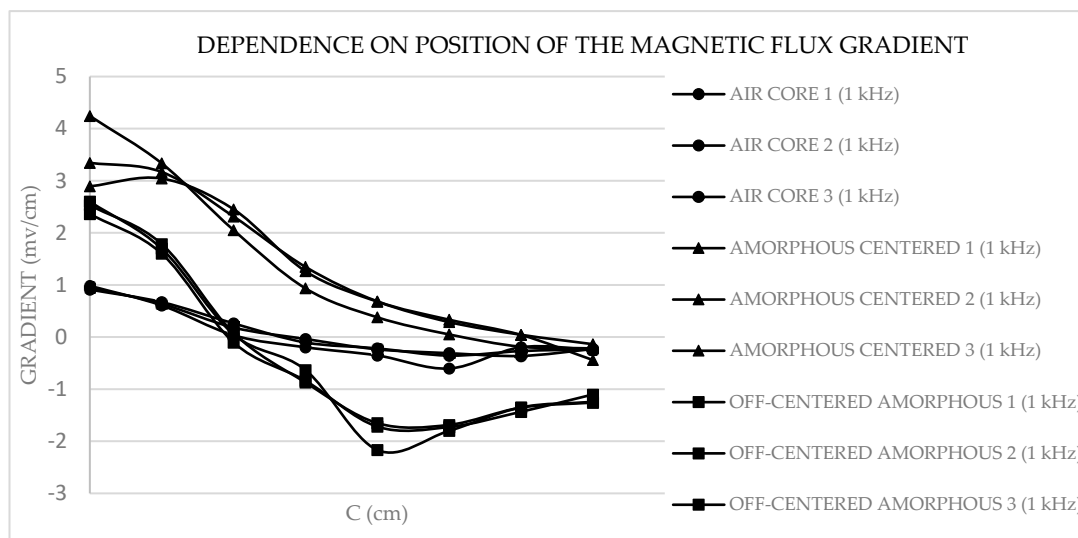

Figure 12. Gradient varying the relative position between primary and secondary coils for 3 different cores in the secondary coil at 1 kHz.

The root cause of the very different results observed in the electromotive force induced in the secondary coil when using an air core and when using an amorphous material core is the permeability of each medium. The permeability of the amorphous material is much higher than the permeability of air [24].

Comparing the results obtained with 10 Hz (Figure 13), a graph similar to the one obtained with 1 kHz was observed (Figure 14); in both cases, the multiplying effect of the amorphous material can be easily appreciated.
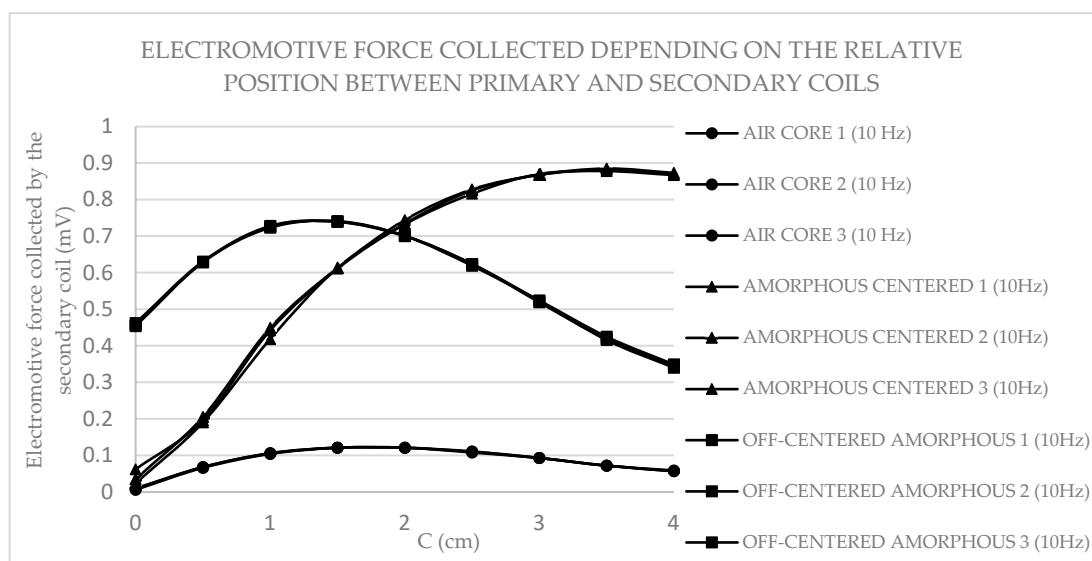
Figure 13. Induced electromotive force varying the relative position between primary and secondary coils for 3 different cores in the secondary coil at 10 Hz.
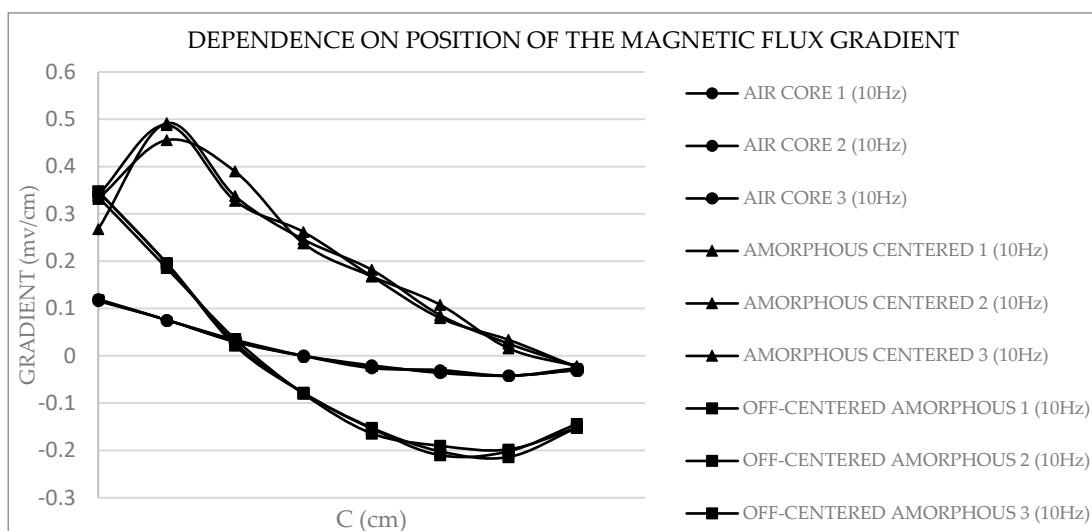

Figure 14. Gradient varying the relative position between primary and secondary coils for 3 different cores in the secondary coil at 10 Hz.

To show all the results in a single graph, the averages of the three tests (P1, P2, P3) performed for each case were calculated in Figure 15.

Taking the numerical value of the maximum gradient of each test and comparing them, it was observed that the maximum value of the gradient corresponded to the test in which the coil was centered with respect to the amorphous material. Therefore, the optimum system to recover the maximum possible energy was the one whose secondary coil had a centered core of amorphous material.

The measurements showed that the ratio between the voltage obtained with the amorphous core (either centered or off-center) and the voltage with an air core, on one side for the 1 kHz tests and on the other side for the 10 Hz tests, was independent of the frequency. This means that the multiplicative effect of the core is independent of the frequency; the magnetic permeability being this multiplicative factor meant that the permeability does not depend on the frequency in the range between 10 Hz and 1 kHz.
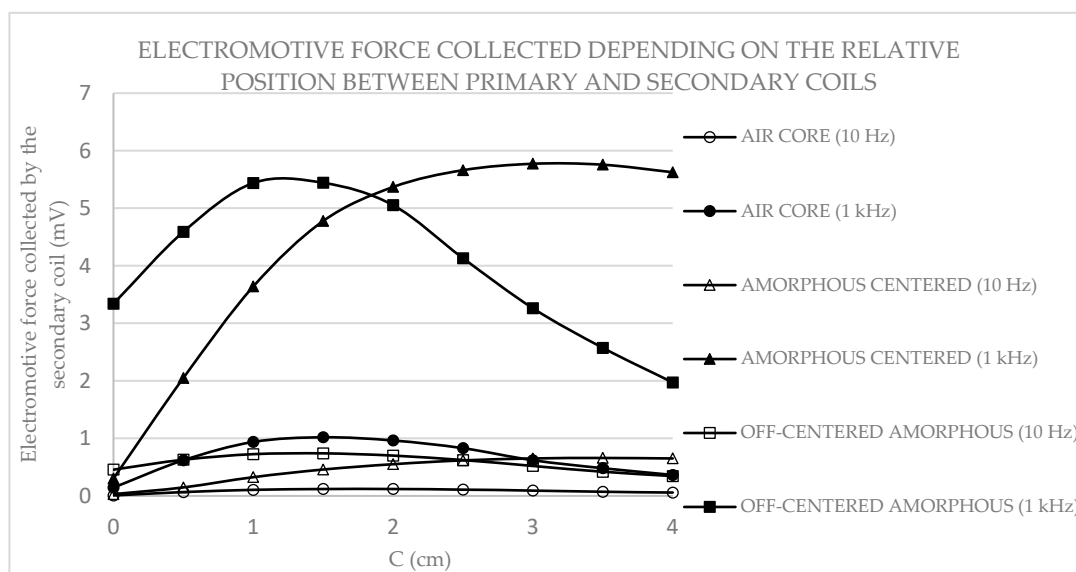
Figure 15. Induced electromotive force from varying the relative position between primary and secondary coils for 3 different cores in the secondary coil at 10 Hz and 1 kHz.

This fits perfectly with different previous observations [24].

In future lines of research, this could be a point of study, trying to find for which frequency the behavior or tendency of these curves changes.

4. Conclusions

As a result of the work and tests carried out, the following conclusions about the proposed system ere obtained.

First and foremost, this article demonstrated that incorporating an amorphous material core into the secondary coil effectively multiplied the magnetic flux by a factor ranging approximately from six to nine times, for frequencies of 10 Hz and 1 kHz, respectively. This substantial increase was clearly visible in Figures 11 and 13, implying that the power was enhanced by approximately 40 to 80 times solely due to the inclusion of the amorphous core.

Furthermore, the experiments were carried out with two different configurations of the amorphous core. On the one hand, with the secondary coil centered on the amorphous core and on the other hand with the secondary coil off-centered, specifically positioned at the end of the films of the amorphous core. Data collection pointed out that by applying the same magnetic field, the flux variation was greater if the coil was centered with the amorphous films' core (as can be seen in Table 4 and Figure 12, where the maximum gradient value was given with this configuration). This is because the effective magnetic field was lower at the ends of the films, as the demagnetizing field was inhomogeneous, and it was greater at the ends of the films. Therefore, the optimum position that maximized the recovered energy was the one corresponding to the secondary coil with the core of amorphous material centered with respect to the coil.

In this study, we opted for Fe-Ni based amorphous ribbons primarily due to their ready availability in our laboratory, and as they serve as a suitable preliminary material to examine the contrast between the system with and without amorphous material, and for the two proposed amorphous material configurations. Looking ahead, future research could focus on optimizing this secondary element, exploring the use of other amorphous materials such as cobalt, considering the annealing of the films, or even experimenting with different core geometries such as microwires.

Table 4. Numerical values of the maximum gradients of each curve.

	Maximum Gradients at 1 kHz			Maximum Gradients at 10 Hz		
	dV/dA (mV/cm)	dV/dA (mV/cm)	dV/dA (mV/cm)	dV/dA (mV/cm)	dV/dA (mV/cm)	dV/dA (mV/cm)
	P1	P2	P3	P1	P2	P3
Air core	0.984	0.912	0.95	0.12	0.118	0.116
Centered amorphous core	4.244	3.344	3.044	0.456	0.488	0.492
Off-centered amorphous core	2.602	2.534	2.364	0.336	0.348	0.348

Lastly, the data obtained at frequencies of 10 Hz and 1 kHz (displayed in Figures 5 and 13) clearly indicate that the permeability maintains a relatively steady state within this frequency range.

Institutional Review Board Statement: Not applicable.

Informed Consent Statement: Not applicable.

Data Availability Statement: No new data were created or analyzed in this study. Data sharing is not applicable to this article.

Conflicts of Interest: The authors declare no conflict of interest.

References

1. Edenhofer, O.; Sokona, Y.; Minx, J.C.; Farahani, E.; Kadner, S.; Seyboth, K.; Adler, A.; Baum, I.; Brunner, S.; Kriemann, B.; et al. (Eds.) *Climate Change 2014 Mitigation of Climate Change Working Group III Contribution to the Fifth Assessment Report of the Intergovernmental Panel on Climate Change*; Cambridge University Press: Cambridge, UK, 2014.
2. Yang, K.; Huang, Y.; Qin, Y.; Hu, C.; Tang, X. Potential and Challenges to Improve Vehicle Energy Efficiency via V2X: Literature Review. *Int. J. Veh. Perform.* **2021**, *7*, 244–265. [CrossRef]
3. Pan, H.; Qi, L.; Zhang, Z.; Yan, J. Kinetic Energy Harvesting Technologies for Applications in Land Transportation: A Comprehensive Review. *Appl. Energy* **2021**, *286*, 116518. [CrossRef]
4. Hamada, A.T.; Orhan, M.F. An Overview of Regenerative Braking Systems. *J. Energy Storage* **2022**, *52*, 105033. [CrossRef]
5. Samn, A.A.; Abdelhaleem, A.M.M.; Kabeel, A.M.; Gad, E.H. Ride Comfort, Road Holding, and Energy Harvesting of a Hydraulic Regenerative Vehicle Suspension. *SAE Int. J. Passeng. Cars Mech. Syst.* **2020**, *13*, 159–171. [CrossRef]
6. Bowen, L.; Vinolas, J.; Olazagoitia, J.L.; Echavarri Otero, J. An Innovative Energy Harvesting Shock Absorber System Using Cable Transmission. *IEEE/ASME Trans. Mechatron.* **2019**, *24*, 689–699. [CrossRef]
7. Gijón-Rivera, C.; Olazagoitia, J.L. Methodology for Comprehensive Comparison of Energy Harvesting Shock Absorber Systems. *Energies* **2020**, *13*, 6110. [CrossRef]
8. Li, Z.; Zuo, L.; Luhrs, G.; Lin, L.; Qin, Y. Electromagnetic Energy-Harvesting Shock Absorbers: Design, Modeling, and Road Tests. *IEEE Trans. Veh. Technol.* **2013**, *62*, 1065–1074. [CrossRef]
9. Aberturas, S.; Hernando, A.; Luis Olazagoitia, J.; Ángel García, M. Study of an Energy-Harvesting Damper Based on Magnetic Interaction. *Sensors* **2022**, *22*, 7865. [CrossRef] [PubMed]
10. Ebrahimi, B. Development of Hybrid Electromagnetic Dampers for Vehicle Suspension Systems. Ph.D. Thesis, University of Waterloo, Waterloo, ON, Canada, 2009.
11. Midgley, W.J.B.; Cathcart, H.; Cebon, D. Modelling of Hydraulic Regenerative Braking Systems for Heavy Vehicles. *Proc. Inst. Mech. Eng. Part D J. Automob. Eng.* **2013**, *227*, 1072–1084. [CrossRef]

12. Gonzalez, A.; Olazagoitia, J.L.; Vinolas, J.; Ulacia, I.; Izquierdo, M. An Innovative Energy Harvesting Shock Absorber System for Motorbikes. *IEEE/ASME Trans. Mechatron.* **2021**, *27*, 3110–3120. [CrossRef]

13. Lee, J.; Choi, B. Development of a Piezoelectric Energy Harvesting System for Implementing Wireless Sensors on the Tires. *Energy Convers. Manag.* **2014**, *78*, 32–38. [CrossRef]

14. Jayakrishnan, E.P.; Sayed, J. Piezoelectric Energy Harvesting: A Review on Power Conditioning. In *Advances in Control Instrumentation Systems*; Springer: Berlin/Heidelberg, Germany, 2020; Volume 660, pp. 1–8. [CrossRef]

15. Ali, A.; Ahmed, A.; Ali, M.; Azam, A.; Wu, X.; Zhang, Z.; Yuan, Y. A Review of Energy Harvesting from Regenerative Shock Absorber from 2000 to 2021: Advancements, Emerging Applications, and Technical Challenges. *Environ. Sci. Pollut. Res.* **2022**, *30*, 5371–5406. [CrossRef] [PubMed]

16. Tang, X.; Lin, T.; Zuo, L. Design and Optimization of a Tubular Linear Electromagnetic Vibration Energy Harvester. *IEEE/ASME Trans. Mechatron.* **2014**, *19*, 615–622. [CrossRef]

17. Zhang, X.; Pan, H.; Qi, L.; Zhang, Z.; Yuan, Y.; Liu, Y. A Renewable Energy Harvesting System Using a Mechanical Vibration Rectifier (MVR) for Railroads. *Appl. Energy* **2017**, *204*, 1535–1543. [CrossRef]

18. Guo, S.; Xu, L.; Liu, Y.; Guo, X.; Zuo, L. Modeling and Experiments of a Hydraulic Electromagnetic Energy-Harvesting Shock Absorber. *IEEE/ASME Trans. Mechatron.* **2017**, *22*, 2684–2694. [CrossRef]

19. Emilio-Bowen, L.; Vinolas, J.; Luis-Olazagoitia, J. Banco de Ensayo Para Validar El Modelo Computacional de Un Cuarto de Coche Con Amortiguador Recuperador de Energía. *Dyna* **2018**, *93*, 82–88. [CrossRef] [PubMed]

20. Sabzehgar, R.; Maravandi, A.; Moallem, M. Energy Regenerative Suspension Using an Algebraic Screw Linkage Mechanism. *IEEE/ASME Trans. Mechatron.* **2014**, *19*, 1251–1259. [CrossRef]

21. Maravandi, A.; Moallem, M. Regenerative Shock Absorber Using a Two-Leg Motion Conversion Mechanism. *IEEE/ASME Trans. Mechatron.* **2015**, *20*, 2853–2861. [CrossRef]

22. Zhang, R.; Wang, X.; Al Shami, E.; John, S.; Zuo, L.; Wang, C.H. A Novel Indirect-Drive Regenerative Shock Absorber for Energy Harvesting and Comparison with a Conventional Direct-Drive Regenerative Shock Absorber. *Appl. Energy* **2018**, *229*, 111–127. [CrossRef]

23. European Commission. European Rare Earth Magnet Recycling Network. EREAN Project. Fact Sheet. FP7. CORDIS. Available online: https://cordis.europa.eu/project/id/607411 (accessed on 20 May 2023).

24. Hernando, A.; Madurga, V.; Barandiarán, J.M.; Liniers, M. Anomalous Eddy Currents in Magnetostrictive Amorphous Ferromagnets: A Large Contribution from Magnetoelastic Effects. *J. Magn. Magn. Mater.* **1982**, *28*, 109–116. [CrossRef]

25. Liebermann, H.H. *Rapidly Solidified Alloys*; CRC Press: Boca Raton, FL, USA, 1993; ISBN 9780429068836.

26. Barandiarán, J.M.; Hernando, A.; Madurga, V.; Nielsen, O.V.; Vázquez, M.; Vázquez-López, M. Temperature, Stress, and Structural-Relaxation Dependence of the Magnetostriction in (Co 0.94/BFe 0.06) 75/BSi 15 B 10. *Phys. Rev. B* **1987**, *35*, 5066–5071. [CrossRef] [PubMed]

27. Hernando, A.; Vazquez, M.; Barandiaran, J.M. Metallic Glasses and Sensing Applications. *J. Phys. E* **1988**, *21*, 1129. [CrossRef]

28. Nielsen, O.V.; Hernando, A.; Madurga, V.; Gonzalez, J.M.; Nielsen, O.V.; Hernando, A.; Madurga, V.; Gonzalez, J.M. Experiments Concerning the Origin of Stress Anneal Induced Magnetic Anisotropy in Metallic Glass Ribbons. *J. Magn. Magn. Mater.* **1985**, *46*, 341–349. [CrossRef]